Angle-resolved photoemission studies of the nickel (111) surface and its interaction with carbon monoxide

P. M. Williams, P. Butcher, and J. Wood*
V. G. Scientific Ltd., East Grinstead, Sussex, England

K. Jacobi
Fritz Haber Institut der Max Planck Gesellschaft, Berlin, Federal Republic of Germany

(Received 8 April 1976)

Angle-resolved photoelectron energy distributions have been recorded for the Ni(111) surface, both clean and following CO adsorption, using He I and He II photons. The results for the clean surface exhibit many features characteristic of an initial-state dependence, but indicate a narrower bandwidth than that inferred from calculated electronic energy band schemes. Qualitatively, the form of the energy-band dispersion predicted from the angular measurements on a simple free-electron-like assumption for the final state, is consistent with the form of the calculated bands and appropriate behavior in the measured dispersion for wave vectors in the vicinity of the Brillouin-zone boundary is observed. However, uncertainties in the component of electron momentum perpendicular to the surface preclude too close a comparison. For the CO-covered surface, comparison of the angular symmetries of the extra structure introduced following adsorption provides a basis for a new assignment in terms of 1π, 5σ, and 4σ molecular orbitals of CO.

I. INTRODUCTION

Nickel has formed the subject of numerous photoemission investigations,[1-19] the essential aim common to all such studies being an increased understanding of the structure of d electrons within the clean metal together with some knowledge of how these d electrons interact with molecular and atomic species during adsorption. The different approaches adopted in these investigations encompass a wide range of experimental conditions, particularly with regard to factors of photon energy and the angular acceptance of the electron energy analyzer, and since photoemission is a multiparameter process depending strongly, under certain circumstances, on such variables as photon energy, it might therefore be anticipated that a consistent overall picture of the electronic structure of nickel would be difficult to deduce from the data. However, on certain key features, such as total d bandwidth there is a consensus of agreement on the empirical interpretation of these results which suggests a possible conflict with some theoretical treatments of the photoemission process.

Classically, one simple approach to the interpretation of photoemitted-electron energy-distribution curves (EDC's) from solids relies on a direct comparison of the EDC with one-electron initial densities of states inferred from band-structure calculations,[20-22] and it is on the basis of these ideas that such a conflict arises in the case of nickel. Of course, features in the one-electron density of states must be weighted by appropriate optical matrix elements involving the final state in the photoemission process, and the many-electron nature of the latter, considered by numerous authors,[23-28] may preclude so literal and simplistic a means of interpretation as this. It is true, for example, that line-shape effects which distort the EDC from a simple one-electron density-of-states profile via many-body effects in the final state have been detected experimentally in core-level asymmetries in x-ray photoelectron spectroscopy.[29] Nevertheless, such perturbing factors, although undoubtedly of interest, may be of secondary importance in the determination of the overall form of the EDC. The overwhelming weight of empirical evidence from photoemission studies of semiconductors, where perhaps more straightforward comparisons with the optically established forms of the densities of states have successfully been made, does indeed suggest that one-electron initial-state band effects should be of considerable relevance in determining at least the qualitative form of the EDC from a transition metal such as nickel.

Again, in the study of adsorbate-metal systems, following the early work of Eastman and Cashion,[11] numerous authors have relied on simple assignments of extra structure, introduced into the clean-metal EDC following controlled adsorption, in terms of a direct comparison with the binding energies of structure within the gas-phase photoemission EDC's from the gas in question. The possible dangers inherent in such an extrapolation have been pointed out elsewhere,[30] however, and in the case of CO on Ni, in particular, Lloyd[31]

first suggested an alternative assignment of structure within the adsorbate EDC based on comparisons with gas-phase spectra of the nickel carbonyls. Theoretical calculations[32] and further synchrotron excited photoemission studies[13] have confirmed Lloyd's analysis, as is considered further below. The identification of structure in EDC's introduced by adsorbates is therefore a subject of some controversy and is not as simple a procedure as originally proposed.

In the majority of measurements to date, interpretations have been hindered by the manner of recording (and hence the information content of) the photoemitted EDC. Although photon energies have been varied over wide ranges and electron energies routinely measured with resolutions of 0.1 eV or so, it is only recently that the great importance of angular effects in photoemitted EDC's from solids has been experimentally demonstrated,[33-43] even though the value of such measurements, in which electron momentum, as well as photon and electron energies, is well specified has been stressed theoretically for a number of years.[23-28] It was the purpose of the present investigation to make a preliminary reexamination of the photoemitted EDC's from a Ni(111) single crystal, clean and following CO adsorption, under conditions of stringent control of the angular acceptance of the electron energy analyzer. The results to be presented provide clear evidence for one-electron band effects in the EDC's at 21.2- and 40.8-eV photon energy, and also give a definitive reassignment of the origins of structure in the EDC following adsorption of CO. These results represent the first well-controlled angle-resolved photoemission measurement of a metal-adsorbate system.

II. EXPERIMENTAL

Measurements were carried out in an ultra high-vacuum electron spectrometer (VG Scientific, model ADES 400) incorporating a windowless discharge uv source (collimated to approximately 1.5 mm at the sample surface), a single crystal manipulator, ion etching and heating facilities, and a hemispherical electrostatic energy analyzer capable of rotation about the axis of primary rotation of the manipulator, and in a plane containing the incident photon beam. A second rotation of the sample around the crystal normal, also contained within this horizontal plane, was provided by the manipulator. The relative zeros of the manipulator and analyzer rotations were easily aligned by viewing light specularly reflected off the crystal surface through a small hole within the analyzer itself. Thus photon incidence angle (ψ) and photoelectron exit polar angle (θ), both measured with respect to the crystal normal, could be accurately and independently set. A circular aperture into the electron energy analyzer defined electron trajectories within a cone of semi-angle $\sim 2^\circ$ at the sample surface. The latter was electrically screened from the analyzer in such a way as to permit field-free drift of the photoelectrons towards the aperture (Mumetal construction of the chamber reduced the residual terrestrial magnetic field at the sample surface to less than 10 mg).

A (111) face of a single crystal of nickel was cut and polished to within 1° or 2° of the desired orientation using standard techniques. Following evacuation and bakeout of the chamber, base pressures below 5×10^{-11} Torr were routinely obtained, and the crystal was cleaned by alternate cycles of argon-ion etching, annealing, and final, short-duration, high-temperature flashing (the same crystal had been extensively degassed and cleaned by oxidation and reduction cycles in earlier studies). The orientation and surface condition could finally be checked by *in situ* low-energy-electron-diffraction (LEED) observations.

During recording of the EDC's with the windowless lamp, pressure in the chamber could be maintained at or below 1×10^{-9} Torr with the lamp optimized for He II (He II:He I ratios of 1:3). The lamp was therefore left on during adsorption of CO to saturation coverage [in excess of 10 langmuires ($1\,\mathrm{L}\equiv10^{-6}$ Torr sec) exposure at room temperature]. Count rates on the 3*d*-band peak for clean Ni were approximately $2\times10^4\ \mathrm{sec}^{-1}$ for He I and $3\times10^3\ \mathrm{sec}^{-1}$ for He II, typical recording times for a 3-eV scan being 100 sec for He I, 300 sec for He II. For the weaker CO-induced levels using He II, 1000-sec scans were employed.

III. RESULTS

Following cleaning and orientation of the crystal, Fig. 1 shows typical EDC's recorded over a 10-eV range from just above E_F (Fermi energy) using He I photons with (inset) the complete spectrum showing the relationship of the primary photoelectrons to the secondary electron background. The crystal azimuth was set so that by variation of polar angle θ, only electrons within one of the three symmetry-related planes of the fcc Brillouin zone containing critical points Γ, L, K, and L were accepted into the energy analyzer. The incidence angle, ψ of the photons is arbitrarily set at 45° in all spectra in the present investigation as only a weak intensity variation of features in the EDC's with ψ could be discerned. Of interest in Fig. 1 is that no significant photoemission inten-

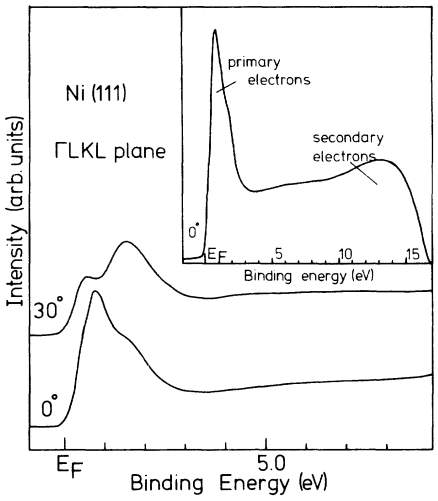

FIG. 1. Angle-resolved energy-distribution curves (EDC's) for a nickel (111) crystal for wave vectors projecting onto the ΓLKL plane of the Brillouin zone. The flat background below the main d-electron structure emphasizes the narrow bandwidth typically observed for Ni in photoemission measurements. Inset, the complete spectrum for normal exit, shows the relationship between primary photoelectron peaks and the secondary electron background. He I excitation.

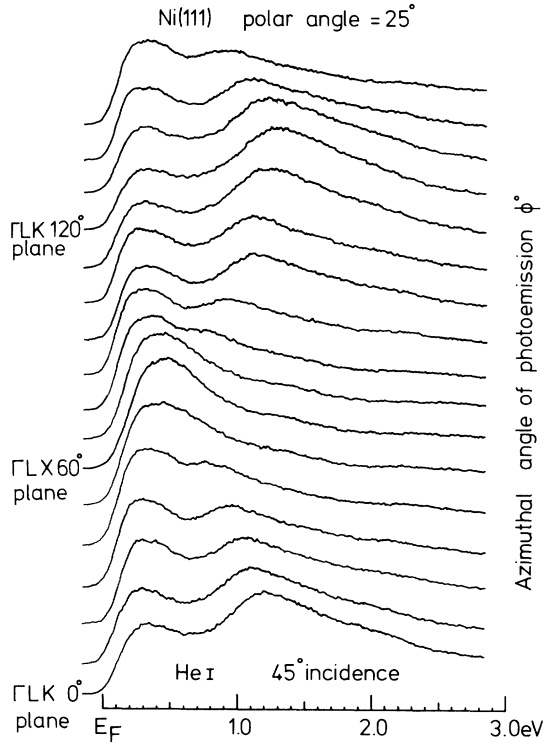

FIG. 2. Azimuthal variation of angle-resolved EDC's for a fixed polar emission angle θ of 25° excited with He I (21.2 eV) radiation incident, as in all figures, at 45°. The reproducibility between EDC's separated by 120° reflects the threefold symmetry of the crystal face. High-symmetry planes in the Brillouin zone, determined from LEED, are indicated.

sity is observed below about 3-eV binding energy, in agreement with the bandwidths determined previously, particularly in x-ray photoelectron spectroscopy (XPS).[8] The background below 3 eV is flat and featureless, and therefore all subsequent EDC's were recorded over an energy span of 3 eV from immediately above E_F.

It is of some relevance to confirm that variations in the photoemitted intensity with angle essentially reflect the crystal symmetry as determined by LEED, and so Fig. 2 shows a series of EDC's recorded by using He I radiation for a fixed polar angle of 25°, but varying the azimuthal setting of the crystal. This form of nested plot, as opposed to a simple polar diagram, favored by many authors, of intensity at a specific binding energy plotted against azimuth, appears to be more useful in that the relationship between bands at different high-symmetry points is revealed at the same time as the rotational symmetry is displayed. Thus Fig. 2, which shows only a selection of data recorded over the full 360°, reveals clearly not only the threefold symmetry of the (111) surface, but also how the extremal excursions of features within the EDC's coincide with low-index planes, in this case containing high-symmetry points Γ, L, K, and Γ, L, U, X, respectively. Ideally, since such a presentation of data contains angle-resolved EDC's for general planes within the Brillouin zone, a full series of nested plots over suitable intervals of polar angle θ might seem the best way in which to proceed. However, since theoretical calculations are generally available only for high-symmetry directions, the present investigation is confined to those high-symmetry planes revealed in the extremal band excursions of Fig. 2.

Thus for a fixed azimuthal setting of the crystal, Fig. 3 shows the polar-angle variation of the EDC's over the same energy range as in Fig. 2, for wave vectors contained within the ΓLKL plane. The separation of the dominant peak near 0.6 eV in the normal-exit EDC ($\theta = 0$) into two components is immediately apparent; less marked is the behavior of the low binding-energy shoulder on the first of these two features in the region $\theta \sim 30°$–$50°$. This shoulder moves up towards the Fermi level between 30° and 35°, crossing the latter somewhere between 35° and 40° before reappearing again at 45°. An expanded series of EDC's (recorded over 1-eV span) between 27.5° and 35°, highlighting this behavior is shown in Fig. 4, from which the discontinuity, around 90 meV wide at 32.5°, can be

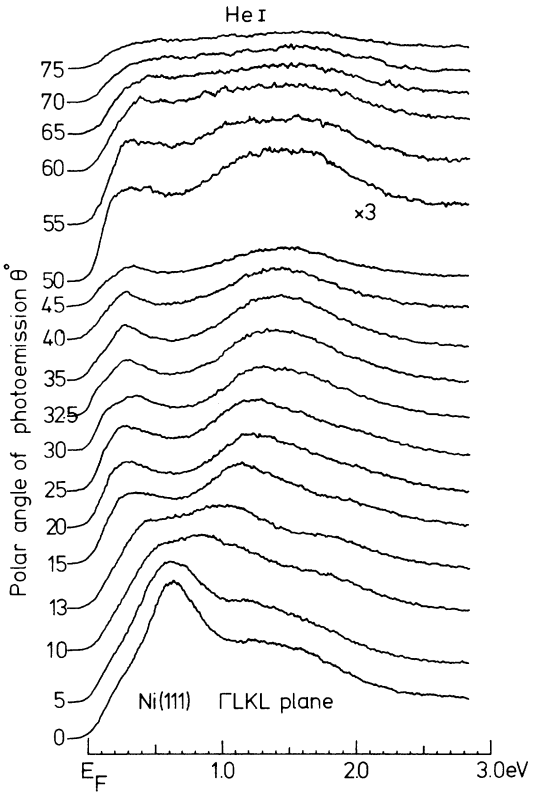

FIG. 3. Polar variation of angle-resolved EDC's for an azimuth projecting onto the ΓLKL plane. He I excitation. Count rate on peak in normal-exit EDC is approximately 2×10^4 sec^{-1}.

seen to be the most distinct feature in all the EDC's; this was therefore used to calibrate the position of the Fermi energy for all the measurements. The overall decrease in intensity with θ,

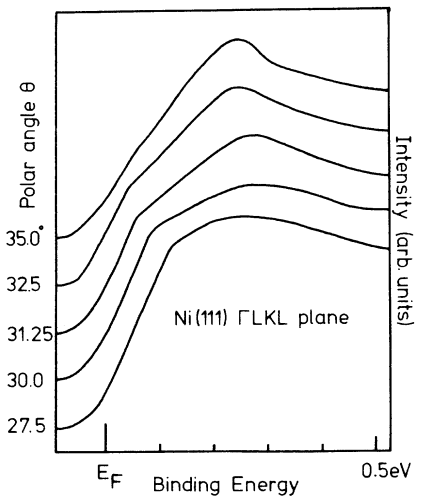

FIG. 4. Series of EDC's for the ΓLKL plane, recorded over an expanded energy range between $\theta = 27.5°$ and 35°, highlighting the movement of the shoulder in Fig. 3 towards the Fermi level.

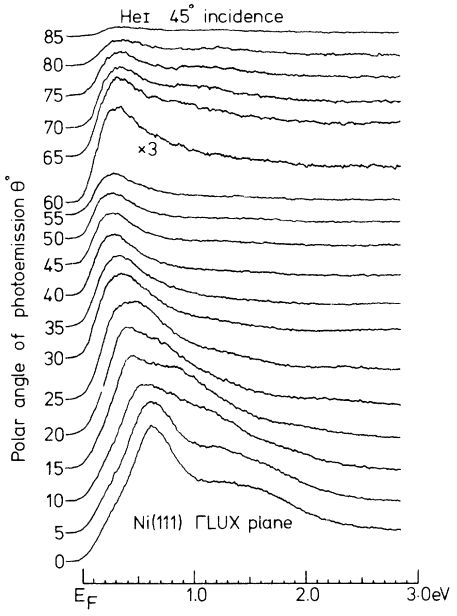

FIG. 5. Polar variation of angle-resolved EDC's for an azimuth projecting onto the ΓLUX plane, at 60° to the series of Fig. 3. He I excitation. Note that the closest excursion of the dominant peak in the EDC's towards the Fermi level occurs near 50°.

observed for most series of EDC's, is as anticipated, and is discussed further below.

Following azimuthal rotation of the crystal by 60° for wave vectors contained with the ΓLUX plane, Fig. 5, we observe entirely different behavior from Fig. 3. Reassuringly, the normal-exit spectra for ΓLKL and ΓLUX series are identical (within the limits of error), confirming the accuracy of orientation of the crystal normal and suggesting that variation of the azimuthal angle of photon incidence (which necessarily accompanies rotation of the crystal about its normal between Figs. 3 and 5) is of negligible importance in the present studies with unpolarized light. Increase in the polar exit angle θ now produces one single peak from the coalescence of the dominant 0.6-eV peak and the broader band near 1.6 eV in the normal-exit spectrum. This single peak exhibits a maximum excursion towards the Fermi level around 50° before moving again to deeper binding energy and, as expected, decreasing in intensity. Similar behavior is observed, Fig. 6, when the photon energy is raised from 21.2 eV (He I) to 40.8 eV (He II), except that the maximum excursion now occurs near 30°. The EDC's are somewhat noisier than those for He I as a result of the lower operating intensity, but there is now the suggestion of a diffuse feature near 2.0 eV, particularly in the 35° EDC, which is not observed at He I. Also the normal-exit EDC is

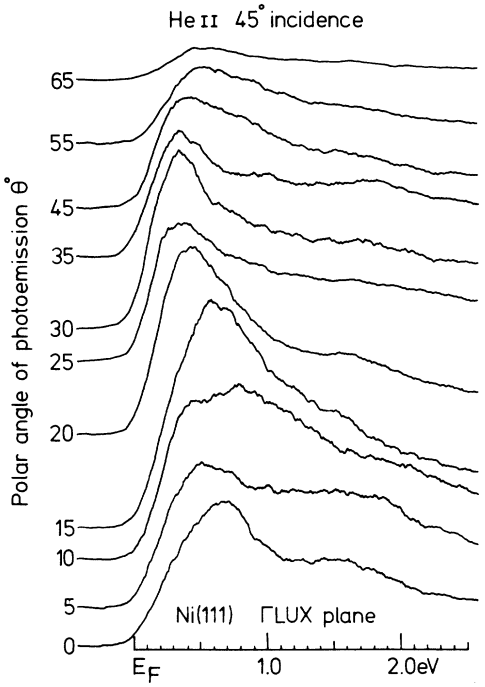

FIG. 6. Polar variation of angle-resolved EDC's for same azimuth as in Fig. 5, but recorded using He II (40.8 eV) excitation. The extremal excursion of the dominant peak now occurs near 30° (cf. Fig. 5).

slightly different, the low binding-energy shoulder below the 0.6-eV peak now being more prominent. Nevertheless, the comparison between He I and He II is close, as discussed further below.

Following the adsorption of CO, peaks now assumed characteristic of the presence of CO from investigations of numerous transition-metal surfaces,[1-19] near 8 and 11 eV appeared in both the He I and He II normal-exit EDC's superimposed on the flat featureless background below the Ni *d* band (cf. Fig. 1). As shown in recent synchrotron measurements[13] the intensity of the 11-eV component relative to that near 8 eV increases considerably between about 20- and 40-eV photon energy, and He II excitation was employed for a detailed study of this structure (which is also, therefore, well removed from the secondary electron "tail" of Fig. 1). Thus Fig. 7 shows the polar-angle dependence of the EDC's between 6- and 12-eV binding energy for an azimuthal crystal setting projecting onto the Γ*LUX* plane of the Brillouin zone. Little azimuthal dependence of the intensity of the CO structure could be observed, so that this plane was chosen somewhat arbitrarily. Considerable dependence of both intensity and binding energy on polar angle θ is observed for both components, the intensity data, after due allowance for background, being summarized in Fig. 8. Thus both pieces of structure first in-

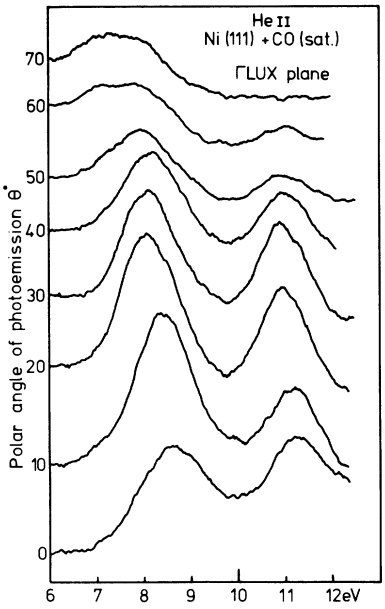

FIG. 7. Polar variation of angle-resolved EDC's for the same azimuth as Fig. 5, but now following adsorption of greater than 10 L of CO, scanning over the energy range 6–12 eV below E_F. Note that the component near 11 eV in the CO-induced structure vanishes for a polar angle of 70°. A prominent low-binding-energy shoulder on the 8-eV component developes after 40°–50° polar angle. Note also the band like variation in the peak position of the 8-eV component between 0° and 40°.

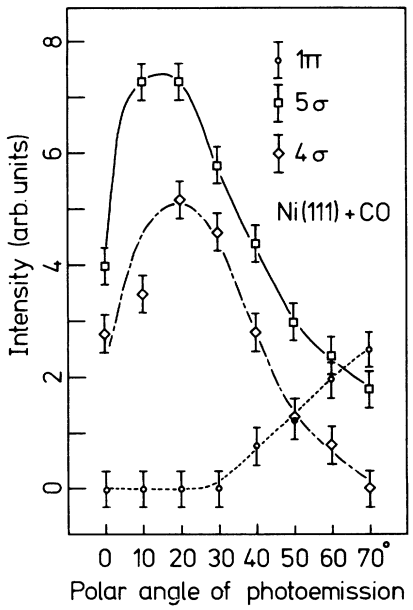

FIG. 8. Summary of the data in Fig. 7, plotting intensity of structure in EDC (after allowance for background) against polar angle. The similarity in behavior of the 8- and 11-eV components is evident.

crease in intensity with θ before rapidly decreasing after 20°, the 11-eV component being undetectable for polar angles greater than 65° or so (in fact for grazing emergence at $\theta \sim 80°$ or greater, little intensity could be detected from either component). A low binding-energy shoulder appears on the 8-eV component at around 40° to 50°, and continues to grow in intensity up to 70°. The shape of 70° spectrum is then similar to that recorded previously in less-well-characterized measurements.[14] Note also that the 8-eV component, particularly, shifts initially to lower binding energy as θ increases; although the 11-eV peak does so to a lesser extent, the peak separation in fact increases from 2.5 eV to 0° to 2.9 eV at 30°. CO adsorption resulted in a decrease in the intensity of structure within the nickel d band, 0–3 eV below E_F, together with some suggestion of a positive contribution between 2 and 3 eV in difference spectra, as observed previously (see Ref. 14, in particular). The angular behavior of the structure was qualitatively similar to that for the clean surface, no new structure appearing; nor was any dramatic quenching of structure in the d band observed, suggesting that the majority of the features between 0 and 3 eV for the clean Ni derive from bulk bands and not surface-state resonances.

IV. DISCUSSION

The interpretation of the very detailed effects outlined in Sec. III presents a complex problem in what must be regarded as a field of investigation as yet in its infancy. In the present account, we will attempt only to provide a preliminary answer to the twin questions posed in Sec. I, namely, whether initial-state one-electron band effects may be discerned within the data for the clean surface, and whether angular photoemission can provide a definitive assignment of molecular-orbital structure for the adsorbate-covered surface. From this point of view, it is convenient to treat the clean-surface results and the CO-adsorbate data separately for the purposes of discussion. First, we make some general observations regarding the measurement of angle-resolved EDC's.

The kinetic energy E of the photoemitted free electron together with an accurate specification of the trajectory of this electron into the energy analyzer (in terms of the polar angle θ and azimuthal angle ϕ) completely specify its wave vector $\vec{p}$, where

$$|\vec{p}| = (2mE/\hbar^2)^{1/2} . \tag{1}$$

The total component of electron momentum parallel to the crystal surface, $p_\parallel$, and the component normal to the surface, p_Z, are thus given by

$$p_\parallel = (2mE/\hbar^2)^{1/2} \sin\theta, \quad p_Z = (2mE/\hbar^2)^{1/2} \cos\theta. \tag{2}$$

Here, we shall be concerned with initial states $|\vec{k}_i\rangle$ and optical transitions to final states $|\vec{k}_f\rangle$ within the solid, so that we need to relate $p_\parallel$ and p_Z to crystal momentum. In practice, if specular refraction of the excited electron on transport across the flat crystal surface is assumed, then $p_\parallel$ is conserved (at least to within a reciprocal-lattice vector) and the parallel component of momentum for the final state $|\vec{k}_f\rangle$ is thus well specified. Direct optical transitions between $|\vec{k}_i\rangle$ and $|\vec{k}_f\rangle$ then determine the initial-state wave vector, again to within a reciprocal-lattice vector. In principle, therefore, since the binding energy E_B of all major structure in the EDC's is known, a map of E_B against $\vec{k}_i$, related to the initial-state one-electron band structure, may be constructed, providing k_Z is also known for the initial state.

However, the determination of k_Z within the crystal presents a greater problem than for $k_\parallel$, as considered by Smith *et al.*[33] in the case of GaAs, and later, the layered solids related to TaS_2.[36] The latter case may readily be analyzed by neglecting k_Z and treating the $E_B \rightarrow k_\parallel$ plot as a two-dimensional projection of the band structure; such an interpretation is valid here since for these materials, the energy bands along k_Z are essentially flat. Such is not the case for GaAs or, in the present investigation, an fcc metal such as nickel. In these cases, a strong band-structure dependence on k_Z is expected, but momentum broadening of k_Z for the final state may obliterate useful information in this type of measurement.[27] For the purpose of the present investigation, we will therefore confine discussion to the behavior of E_B related to $k_\parallel$ and examine whether such a two-dimensional projection of the energy bands may usefully be compared with calculated schemes.

The geometrical dispersion of such projected energy bands may by these means easily be specified, but thus far, nothing has been discussed with regard to the atomic character of the wave functions comprising these bands, or the optical transitions between initial and final states. At this point, available theoretical accounts of the photoemission process tend to diverge. Liebsch[45] stresses the importance of scattering in the final state $|\vec{k}_f\rangle$ as a determining factor in the behavior of angle-resolved EDC's. The approach of Gadzuk[46] and Grimley,[47] however, emphasizes the role of the initial state in determining at least the symmetries of angle-resolved photoemitted intensity distributions. Briefly, following the latter, if we

assume a tight-binding sum for the initial state $|\vec{k}_i\rangle$ then

$$|\vec{k}_i\rangle = \sum_j \phi(\vec{r} - \vec{R}_j) e^{i\vec{k}_i \cdot \vec{R}_j}, \tag{3}$$

the sum being taken over lattice sites R_j; $\phi(\vec{r})$ represent atomic orbitals (or appropriate sums of atomic orbitals in the case of a CO adsorbate). Representing the photoelectron as a plane wave $e^{i\vec{p}\cdot\vec{r}}$, it is now assumed that this same function describes the final state $|\vec{k}_f\rangle$ within the crystal. The optical transition rate [and hence the contribution $I(\vec{p})$ to the intensity of photoelectrons of wave vector $\vec{p}$] between $|\vec{k}_i\rangle$ and $|\vec{k}_f\rangle$, proportional to $|\langle k_f|\vec{A}\cdot\vec{\nabla}|k_i\rangle|^2$, may then be simply valuated; this, of course, neglects terms in $\vec{p}\cdot\vec{A}$ in the matrix element which, it has recently been suggested,[38] may account for a certain contribution to the photoemitted intensity from tungsten at photon energies below the plasma frequency. For radiation of a single fixed polarization and vector potential $\vec{A}$, we then find

$$I(\vec{p}) \sim A^2 p^2 \cos^2\beta |\phi(\vec{p})|^2 \times \delta(E_f - E_i - \hbar\omega) \sum_G \delta(\vec{k} - \vec{G} - \vec{p}), \tag{4}$$

where the δ functions conserve energy and momentum, respectively, and

$$\phi(\vec{p}) = \int e^{i\vec{p}\cdot\vec{r}} \phi(\vec{r})\, d^3r \tag{5}$$

is simply the momentum representation of the atomic orbital. The angle between $\vec{A}$ and $\vec{p}$ is β, but note that in the present investigation, the average value $\langle \cos^2\beta \rangle$ is required, since unpolarized radiation is employed: this term leads to the monotonic falloff in intensity in the majority of series of EDC's as θ (and hence $\langle \beta \rangle$) increases. The second term in Eq. (5), in $|\phi(\vec{p})|^2$, determines the symmetry dependence of the photoemitted intensity and emphasizes the role of the initial state $\phi(\vec{r})$ (rather than the final state $|\vec{k}_f\rangle$) in this respect. Note also that the δ function in energy is a factor by no means to be neglected; the constraint of energy conservation forms the requirement that for all photon energies and initial-state binding energies and momenta, an allowed final state (here represented by $e^{i\vec{p}\cdot\vec{r}}$) may be found. Although momentum broadening in the final state[27] may be thought of as relaxing this condition somewhat, at the photon energies in the present investigation (He I and He II) recent studies of graphite[48] indicate that at the lower photon energy particularly, the unavailability of an allowed transition can lead to the photoemitted intensity vanishing for certain wave vectors. Nor is it clear to what extent momentum broadening may inhibit a precise definition of the initial-state wave vector, unless all effects occur in k_z and not in $k_\parallel$.

A. Clean nickel (111) surface

Figures 9 and 10 show the data of Figs. 3–6 reduced to wave-vector–binding-energy diagrams for the ΓLKL and ΓLUX planes, respectively. The dashed boundaries in both figures represent the values of parallel wave-vector component required to reach the Brillouin-zone boundary at K, X, and L, assuming k_z is of the required value in each case. The latter point is stressed further in Fig. 11, which shows a projection of the extended fcc Brillouin zone, the directions of k_z and $k_\parallel$ for the (111) face being indicated. Note that the two planes of interest, containing high-symmetry points Γ, L, K, L and Γ, L, U, X, respectively, conveniently coincide in these diagrams, even though the symmetry-related ΓLUX plane at 120° was in fact selected in the measurement. It is seen that whereas the $k_\parallel$ value required to reach K is unique, the values required to reach X and L are identical. Inset in Figs. 9 and 10, for comparison, are relevant sections of the energy bands for ferromagnetic nickel calculated by Callaway[22] (reproducing only the majority-spin band for simplicity).

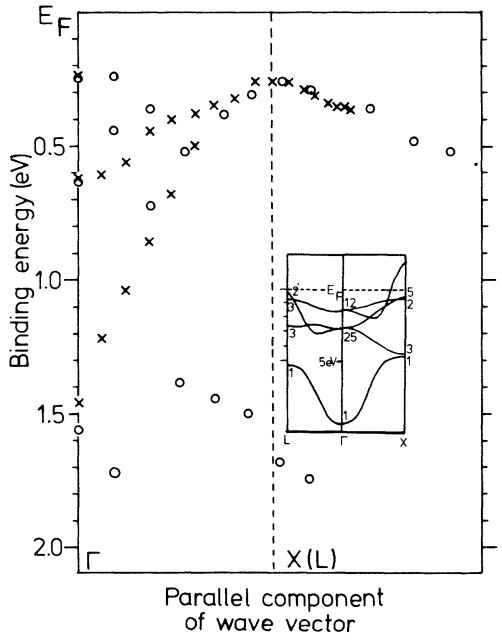

FIG. 9. Variation of binding energies of structure in Figs. 5 and 6 with parallel component of wave vector (ΓLUX plane). Dashed line indicates value of $k_\parallel$ required to reach high-symmetry point X (or L). Inset shows portion of majority-spin bands for ferromagnetic nickel (Ref. 22). Crosses ($\times$)—He I data; circles ($\circ$)—He II.

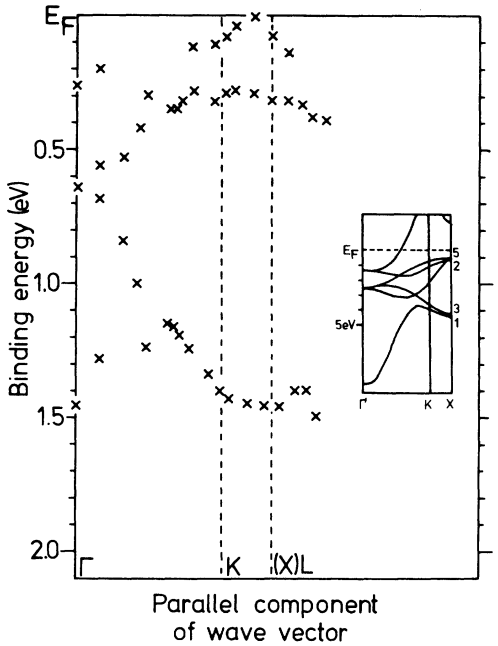

FIG. 10. Binding-energy–wave-vector plot similar to Fig. 9, but for data in Figs. 3 and 4 (ΓLKL plane). Dashed lines again indicate value of $k_{\parallel}$ required to reach K and L (or X).

Before considering in detail these empirical "energy bands" several general points merit attention. As mentioned in Sec. III, the bandwidth of around 2.5 eV (for both He I and He II EDC's, in good general agreement with other measurements,[1-19] is again narrower than anticipated on the basis of calculated band schemes. Although no contribution at these photon energies is expected from the deeper, purer s-like bands below 4 eV

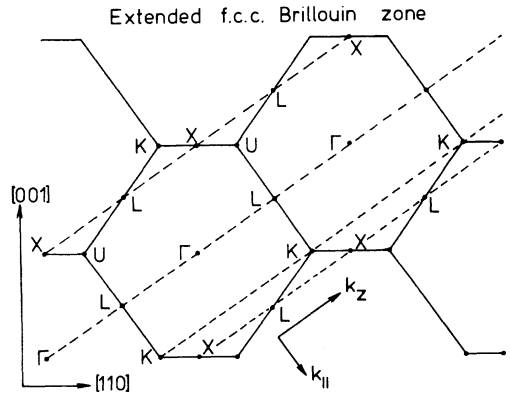

FIG. 11. Schematic of the extended Brillouin zone for fcc structure [$(1\bar{1}0)$ projection] emphasizing that although $k_{\parallel}$ values may be accurately specified (same dashed lines as in Fig. 9 and 10) uncertainty in k_z can lead to contributions from more than one high-symmetry point (e.g., X and L) for same $k_{\parallel}$ value in angle-resolved EDC's.

or so, as a consequence of low photoionization cross sections, there is still a fair discrepancy in the d bandwidth. Since this bandwidth was insensitive to photon incidence angle, we can discount any simple explanation of this fact in terms of weaker excitation of d states of certain symmetries as a result of dependence on polarization via $\vec{A}\cdot\vec{p}$ terms in the optical matrix elements. Clearly, any future experiments with well-polarized radiation and angular resolution will be of considerable interest, but for the present, we must take this and other investigations[1-19] as establishing the empirical fact of a bandwidth near 2.5 eV. Nickel is, of course, ferromagnetic at the temperatures in this, and the majority of other, measurements and this fact should be borne in mind since the exchange-interaction splitting of many bands may be as large as 0.4–0.5 eV. However, this may be expected to broaden features in the EDC's and can in no way account for the bandwidth discrepancy. Mechanisms for the latter in terms of many-body effects in the final state $|\vec{k}_f\rangle$, the fast photoelectron, and the d-band hole coupling strongly to low-energy electron-hole pairs around the Fermi level, would again seem more likely to lead increased bandwidths. Narrowing of energy bands due to surface relaxation is predicted on certain theoretical models[44] but again the magnitude of the discrepancy (up to 3 eV) cannot at present satisfactorily be accounted for on such a basis. Surface-state behavior would appear to be inconsistent with the adsorption data, and for bulk d bands, if present below 3 eV, at some wave vectors, particularly in the vicinity of a zone boundary for either He I or He II excitation, some detectable contribution to the EDC would be anticipated, notwithstanding the constraints placed upon the optical transitions by the δ function in Eq. (4).

With the above observations in mind, we note the following with reference to the bands of Figs. 9 and 10. For the ΓLUX plane, it is of interest to note the exact coincidence in wave vector at the extremal excursion of the uppermost band with that required to reach the zone boundary at X (or L), the latter parameter having been independently inserted from tabulated crystallographic spacings. This coincidence occurs for both He I and He II excitation and indeed the general level of agreement between data for the two photon energies is excellent, strongly suggesting that we are dealing primarily with *initial-state* band positions. Of course, diffraction of the outgoing final-state electron $|\vec{k}_f\rangle$ is expected to give rise to some critical behavior at the same wave-vector values.[45] However, final-state-scattering-based theories invariably predict *intensity* enhancement at these wave vectors, contrary to the observation in the

present case where the peak intensity decreases smoothly and monotonically through the critical wave vector (Fig. 5, although there is some fluctuation at lower $k_{\parallel}$ values in the He II spectra, Fig. 6). As a working hypothesis, therefore, we propose that the band diagram does indeed represent initial states.

At this point, unfortunately, lack of knowledge of k_Z becomes a problem. With references to Fig. 11, k_Z values at the critical $k_{\parallel}$ wave vector of Fig. 9 near either X or L for He I and He II are possible. A reduced-zone scheme could thus place wave-vector values at the two photon energies in the vicinity of different critical points in the first zone with the same $k_{\parallel}$ value, perhaps fortuitously, although umklapp processes might lead to contributions from other high-symmetry points along $\vec{z}$. However, the near identical reproducibility between He I and He II bands suggests more than mere chance coincidence with high-symmetry points, and clearly prompts further measurements over a wider range of photon energies.

For the present, we tentatively suggest that the energy-band plots of Figs. 9 and 10 do map initial-state energy bands along high-symmetry directions between critical points (and not along a general, complex direction). Qualitative comparison with the calculated energy bands does indeed suggest a strong similarity between the measured dispersion and that of Γ_{12} and Γ_{25} bands along ΓX. Bearing in mind that in the normal-exit EDC, we might expect (without further knowledge of the behavior of k_Z) contributions from both Γ and L, such a comparison would place the average positions at Γ (in the sense of the mean position for the majority- and minority-spin bands) of the Γ_{12} and Γ_{25} bands at 0.6 and 1.5 eV below E_F, respectively, the uppermost band in the normal-exit EDC corresponding to L_{32}, L_3 being nearly degenerate in energy with Γ_{25}. At the zone boundary in Fig. 9, the uppermost group then corresponds to the triply degenerate $X_{2,5}$ group of d bands. At X, however, the d bands should be split into manifolds containing six $X_{2,5}$ and four $X_{3,1}$ electrons, respectively, but no conclusive evidence is found for the deeper-lying $X_{3,1}$ feature (with the exception of the ill-defined band around 1.5 eV observed with the He II). Of course, the introduction of strong s character into the bands near X, producing the hybridization gap between X_3 and X_1 may result in a low photoionization cross section. This latter point emphasizes the fact that the atomic character of the initial-state wave functions must inevitably be taken into account in such analyses; geometrical comparison of the energy bands, as in the present investigation, can only provide a preliminary interpretation of features in angle-resolved EDC's. The conclusion to be drawn from the present detailed arguments, however, and from the general observations noted above, is that the energy bands calculated for nickel are too broad, perhaps by as much as 2 eV.

Applying a similar analysis to the data in Fig. 10, a degree of self-consistency is introduced if the two strong bands which develop towards the zone boundary are associated with the $L_{3,2}$ and L_3 bands, respectively; the L critical point would be expected to be reached by these wave vectors. The dispersion of the uppermost band (the shoulder in the data of Figs. 3 and 4) is then consistent with the calculated behavior near L, where the L_3 (majority spin) and L_2 (majority spin) bands cross the Fermi level. At K, no distinct features are expected from the dispersion of the calculated energy bands, in agreement with observation. Again, the present treatment implies much smaller band separations than those calculated, but it should be emphasized once more that these conclusions remain tentative and await confirmation when further data and theoretical treatments are available.

B. Ni(111)-CO-adsorbate surface

Somewhat paradoxically, the CO-covered Ni(111) surface presents, in many respects, a simpler problem with regard to interpretation than the clean-nickel d-band behavior. Here we are concerned primarily with the atomic character of the states in question, and less so with the bandlike dispersion of features in the EDC's (although these latter effects do most certainly occur in the adsorbate resonances, as noted previously). In this context, it is the intensity variation of features in the angle-resolved EDC's as θ varies which is of importance, and with reference to Figs. 7 and 8, we note the following: (i) Three pieces of structure deriving from the presence of CO are clearly discerned in the energy range 6–12 eV, as pointed out by other authors.[12–15] (ii) The intensity behavior with θ of the two main features present in the normal-exit spectrum near 8 and 11 eV is qualitatively identical. The third piece of structure, of lowest binding energy, has a significant intensity only at high polar angle.

At this point, it is convenient to review briefly the previous interpretations of the origins of such structure in light of these present observations. As outlined in the Introduction, the original assignment of the two dominant features in the EDC's to the 5σ and 1π molecular orbitals of the CO, ignoring the 4σ state, has been reversed on the basis of synchrotron cross-section measurements[13] and on preliminary angular experiments for the Ru-CO

system,[49] following suggestions by Lloyd.[31] The deeper binding-energy component is now clearly associated with the 4σ molecular orbital of CO, and the upper feature near 8 eV with a doublet structure contains contributions from the 5σ and 1π orbitals, the component of *deeper* binding energy being due to the 1π. Alternative suggestions, on the basis of one recent self-consistent-field–$X\alpha$ calculation,[50] that the 8-eV peak derives from the 1π state and the 11-eV from the 5σ would appear to be discountable as the 4σ state is again omitted.

Assuming therefore, as a test model, the synchrotron assignment of structure to 5σ, 1π, and 4σ, respectively, in order of increasing binding energy, observation (i) above is clearly explained. The second observation regarding the intensity behavior of the two dominant peaks in the normal-exit spectrum is, however, clearly *inconsistent* with this. With reference to Eq. (5), it is the momentum density distribution $\phi(\vec{p})$ which determines the symmetry dependence in the photoemitted intensity, and observation (ii) implies identical symmetries in $\phi(\vec{p})$ for these two features. Whereas the 4σ and 5σ orbitals exhibit momentum densities which are similarly axially symmetric with respect to the C-O linear bond, the 1π state derives from a weak π-like overlap of $2p$ atomic orbitals of the C and O *normally oriented* with respect to the C-O axis. On such a basis, it may therefore be concluded that if the deep-lying component near 11 eV is associated with the 4σ state, the lower binding-energy component near 8 eV in the normal-exit EDC *must* derive from the 5σ orbital. The 1π level is then observed only at high polar angles and is associated with the lowest binding-energy feature, as summarized in Fig. 12. The relative positions of the three orbital components in this assignment is then consistent with behavior predicted for CO on Ni(100) in a recent molecular-cluster study[32(a)] which shows the 5σ orbital energy below that of the 1π but above the 4σ for certain CO-Ni separations. More recent $CO(Ni)_5$ cluster calculations[32(b)] also yield a similar ordering, in excellent agreement with the present data.

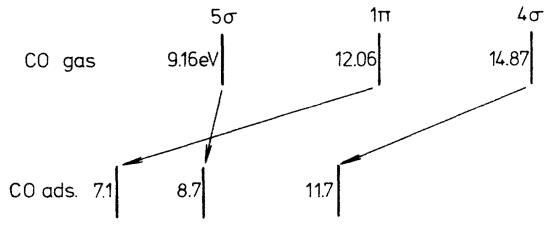

FIG. 12. Energy levels of molecular CO in the gas phase (from Ref. 52) referred to Fermi level (assuming work function to be 4.85 eV) compared with binding energies of features in angle-resolved EDC's from Ni–CO-adsorbate system. The new assignment of features is based on their polar angular dependences (of Figs. 7 and 8); the binding energy of the 1π component is inferred from the 70° EDC of Fig. 7.

The angular behavior shown here for the 1π and for the 5σ and 4σ derived levels is identical with that predicted recently by Grimley[47] for angular variations in photoemission from adsorbed atoms, particularly in such features as the initial *increase* in intensity with θ for the 4σ and 5σ, if we assume the CO molecule to be molecularly adsorbed in an orientation with the C-O axis normal to the nickel surface, as shown in Fig. 13. Such a conclusion leads to strong interaction between the 5σ orbital (which extends predominantly away from the carbon atom) and the nickel d electrons, as pointed out by Doyen and Ertl.[51] Under such circumstances, the energy shifts between the gas phase and adsorbate states in Fig. 12 may readily be accounted for: both the 1π and 4σ orbitals, relatively uninvolved in the bonding, undergo similar relaxation shifts (4.9 and 3.2 eV respectively) on adsorption. The 5σ level is, however, *lowered* in energy relative to these two as a result of strong participation in the chemisorption bond; this latter observation may also account for the marked bandlike dispersion in peak position of the 5σ structure in Fig. 7. We note finally that although the relative intensities of the 5σ and 1π components might seem inconsistent with the simple numerical electron occupancy of these orbitals, conclusions based on this latter numerical parameter are often invalid in angle-resolved measurements. For example, in angular studies of graphite[48] the photoemitted intensity from the $2p_z$ derived bands, with atomic orbitals normal to the (0001) crystal surface, is considerably greater than the contribution from the main $2p_{x,y}$ band, with three times the number of electrons, derived

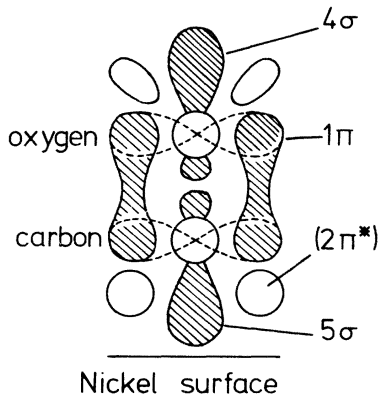

FIG. 13. Schematic of molecular orbitals for CO adsorbed on a nickel surface in a normal orientation. The main 3σ bonding orbital (between the C and O) is not shown.

from in-plane σ overlap between $2p$ orbitals parallel to the crystal surface.

V. SUMMARY

The present investigation has revealed a pronounced angular dependence in the photoemitted energy-distribution curves for the Ni(111) surface, both for clean and CO-saturated states, using both He I and He II photons. For the clean surface, certain trends in the observed photoemission data suggest that an interpretation of features within the EDC's in terms of initial-state one-electron band effects may be appropriate, in particular the relatively weak photon energy dependence and the consistency between wave-vector-dependent criticalities and crystallographically determined zone-boundary positions. Accordingly, a comparison has been made between a calculated band structure for nickel and an empirical scheme based on the dependence of binding energies of features within the EDC's on their momentum components parallel to the crystal surface. Such a plot is essentially a two-dimensional projection of the energy bands and without further knowledge of the nature of the processes which determine the component of momentum perpendicular to the crystal surface, only a preliminary identification of features in the EDC's with critical symmetry points in the calculated bands may be made. Nevertheless, a positive consequence of this initial-state analysis is that calculated bandwidths for nickel appear to have been overestimated. Further angle-resolved experiments to test this hypothesis using (110) and (100) oriented Ni crystals are planned.

For the CO-saturated surface, the now familiar adsorbate-induced features near 8 and 11 eV are observed in the EDC's for both He I and He II photons. Considerable intensity variation with the polar angle of emission is observed for both using He II excitation, the behavior of the deeper component near 11 eV being consistent with its identification as deriving from the 4σ molecular orbital of CO in recent synchrotron excited photoemission investigations. For a normally oriented CO molecule this assumes, as for the clean surface, that it is the momentum density in the initial state which determines the observed symmetries. Comparison of the relative intensity dependence with angle for both components then suggest a clear assignment of the dominant feature near 8 eV to the 5σ orbital, not the 1π orbital as suggested previously. The latter appears as a low binding-energy shoulder on the 5σ structure only at high polar angle. This new assignment of the orbital structure for adsorbed CO on nickel is consistent with a recent cluster calculation and with the relaxation and bonding shifts expected if the 5σ orbital provides the dominant contribution to the Ni-CO chemisorption bond.

---

*Present address: Dept. of Inorganic Chemistry, Chalmers University of Technology, Gothenburg, Sweden.

[1]A. J. Blodgett and W. E. Spicer, Phys. Rev. 146, 390 (1966).
[2]D. E. Eastman, J. Appl. Phys. 40, 1387 (1969).
[3]D. E. Eastman, J. Phys. (Paris) 32, C1-293 (1971).
[4]D. E. Eastman and W. F. Krolikowski, Phys. Rev. Lett. 21, 623 (1968).
[5]T. A. Callcott and A. U. Macrae, Phys. Rev. 178, 966 (1969).
[6]Y. Baer, P. F. Heden, J. Hedman, M. Klasson, C. Nordling, and K. Siegbahn, Phys. Scr. 1, 55 (1970).
[7]D. T. Pierce and W. E. Spicer, Phys. Rev. Lett. 25, 581 (1970).
[8]P. J. Page, D. L. Trimm, and P. M. Williams, Trans. Faraday Soc. 1, 70 (1974).
[9]P. J. Page and P. M. Williams, Discuss. Faraday Soc. 58, 80 (1974); 58, 1769 (1974).
[10]P. J. Page and P. M. Williams, in *Vacuum Ultra-Violet Radiation Physics*, edited by E. Koch, R. Haense, and C. Kurz (Pergamon, New York, 1974), p. 566.
[11]D. E. Eastman and J. K. Cashion, Phys. Rev. Lett. 27, 1520 (1971).
[12]C. R. Brundle, J. Electron Spectrosc. 7, L1 (1975).
[13]T. Gustafsson, E. W. Plummer, D. E. Eastman, and J. L. Freeouf, Solid State Commun. 17, 391 (1975).
[14]D. E. Eastman and J. E. Demuth, Jpn. J. Appl. Phys. Suppl. 2, Pt. 2, 827 (1974).
[15]G. E. Becker and H. D. Hagstrum, J. Vac. Sci. Technol. 10, 31 (1973).
[16]R. W. Joyner and M. W. Roberts, Trans. Faraday Soc. 1, 1819 (1974).
[17]C. R. Brundle and A. F. Carley, Trans. Faraday Soc. (to be published).
[18]C. R. Brundle, *Proceedings of the Nato Advanced Study Institute* (Plenum, New York, 1976).
[19]P. R. Norton, R. L. Tapping, and J. W. Goodale, Chem. Phys. Lett. (to be published).
[20]L. Hodges, H. Ehrenreich, and N. D. Lang, Phys. Rev. 152, 505 (1966).
[21]E. I. Zornberg, Phys. Rev. B 1, 244 (1970).
[22]J. Callaway and C. S. Wang, Phys. Rev. B 7, 1096 (1973).
[23]E. O. Kane, Phys. Rev. Lett. 12, 97 (1964).
[24]G. D. Mahan, Phys. Rev. B 2, 4334 (1970).
[25]C. Caroli, D. Lederer Rozenblatt, B. Roulet, D. Saint-James, Phys. Rev. B 8, 4552 (1973).
[26]W. L. Schaich and N. W. Ashcroft, Phys. Rev. B 3, 2452 (1971).
[27]P. J. Feibelman and D. E. Eastman, Phys. Rev. B 10, 4932 (1974).
[28]S. Doniach and M. Sunjic, J. Phys. C 3, 285 (1970).
[29]N. J. Schevchik, Phys. Rev. Lett. 33, 1336 (1974).
[30]D. R. Penn, Phys. Rev. Lett. 28, 1041 (1972).

[31]See remarks of D. R. Lloyd, Discuss. Faraday Soc. 58, 136 (1974).
[32](a) J. T. Waber, H. Adachi, F. W. Averill, and D. E. Ellis, Jpn. J. Appl. Phys. Suppl. 2, Pt. 2, 695 (1974); (b) I. P. Batra and P. S. Bagus, Solid State Commun. 16, 1097 (1975).
[33]N. V. Smith and M. M. Traum, Phys. Rev. Lett. 31, 1247 (1973).
[34]M. M. Traum, N. V. Smith, and F. J. DiSalvo, Phys. Rev. Lett. 32, 1241 (1974).
[35]T. Gustafsson, P. O. Nilsoon, and L. Wallden, Phys. Lett. 37A, 121 (1974).
[36]N. V. Smith and M. M. Traum, Phys. Rev. B 11, 2087 (1975).
[37]R. H. Williams, J. M. Thomas, M. Barber, and N. Alford, Chem. Phys. Lett. 17, 142 (1972).
[38]W. F. Egelhoff and D. L. Perry, Phys. Rev. Lett. 34, 93 (1975).
[39]P. M. Williams, D. Latham, and J. Wood, J. Electron Spectrosc. 7, 281 (1975).
[40]D. R. Lloyd, C. M. Quinn, N. V. Richardson, and P. M. Williams, Commun. Phys. 1, 11 (1975).
[41]D. R. Lloyd, C. M. Quinn, and N. V. Richardson, J. Phys. C 8, L371 (1975).
[42]D. R. Lloyd, C. M. Quinn, and N. V. Richardson, Trans. Faraday Soc. I (to be published).
[43]R. J. Himpsel and W. Steinmann, Phys. Rev. Lett. 35, 1025 (1976).
[44]P. Fulde, A. Luther, and R. E. Watson. Phys. Rev. B 8, 440 (1972).
[45]A. Liebsch, Phys. Rev. Lett. 32, 1203 (1974); A. Liebsch and E. W. Plummer, Discuss. Faraday Soc. 58, 19 (1974).
[46]J. W. Gadzuk, Surf. Sci. 58, 19 (1975).
[47]T. B. Grimley, Discuss. Faraday Soc. 58, 1 (1974).
[48]P. M. Williams (unpublished).
[49]J. C. Fuggle, M. Steinkilberg, and D. Menzel, Solid State Commun. (to be published).
[50]I. P. Batra and O. Robaux, J. Vac. Sci. Technol. 12, 242 (1975).
[51]G. Doyen and G. Ertl, Surf. Sci. 43, 197 (1974).
[52]D. W. Turner *et al.*, *Molecular Photoelectron Spectroscopy* (Wiley, New York, 1970), p. 34.